BEYOND SPATIAL RESOLUTION: COMPARING SENTINEL-2 AND PLANETSCOPE IMAGERY FOR EFFICIENT REMOTE MAPPING

Murilo H. S. de Oliveira[1], Marlon F. de Souza[2*], Fernando K. I. Fugihara[1], Rubens A. C. Lamparelli[1]

[1]Plasticulture Engineering Center, Universidade Estadual de Campinas
[2]Luiz de Queiroz College of Agriculture (ESALQ), University of São Paulo
*marlon.souza@usp.br

ABSTRACT

The choice of remote sensing imagery is critical for balancing accuracy and computational cost in remote sensing applications. This study compares Sentinel-2 (S2) and PlanetScope (PS) satellite imagery for mapping Agricultural Plastic Structures (APS). We investigated the trade-off between PS's higher spatial resolution and the computational demands associated with its larger data volume, using seven machine learning classifiers. Results show that S2 imagery with 10 spectral bands consistently outperformed PS, achieving, on average, 2.5% higher overall accuracy. Crucially, PS image classification took nearly 10x longer, primarily due to the input file size. These results reveal a key scalability challenge: the small increases in accuracy from using more detailed data sources and complex models can become limiting when deploying large-scale mapping. We conclude that S2 imagery is a suitable source for cost-effective, scalable APS mapping using traditional ML classifiers. Our contribution is to elucidate certain aspects of the APS mapping, including runtime as a comparative metric. Future work should explore deep learning models on these image datasets.

1 INTRODUCTION

The choice of image dataset and machine learning (ML) algorithm directly affects the accuracy and computational cost of land cover (LC) classification (Sheykhmousa et al., 2020; Zhang et al., 2025; Li et al., 2022). Selecting a suitable and effective imagery source is not straightforward because, in RS image classification, four key resolutions must be considered: spatial, spectral, temporal, and radiometric. Sentinel-2 (S2) and PlanetScope (PS) are among the most widely used collections, each offering distinct advantages and disadvantages. Since 2018, at least 18 studies have compared PS and S2 imagery for LC classification (LCC), so this comparison is neither novel nor groundbreaking in contemporary research (Basheer et al., 2024). However, the results remain inconclusive regarding which collection yields better outcomes.

This study aims to test whether PS's higher spatial resolution, associated with the recent incorporation of additional spectral bands, may yield improved classification results than S2. We conducted this comparison in a challenging and little-explored case: mapping agricultural plastic structures (APS). We assessed key factors for effective LCC, aiming for a balanced trade-off between accuracy and runtime. Previous studies have discussed little about the scalability required for LCC across extensive geographic areas. This gap underscores the need for an evaluation that accounts for both accuracy and runtime performance in LC mapping workflows. Using large datasets with numerous predictor variables and high spatial resolution raises concerns about optimizing processing to reduce computational costs (Akkiraju et al., 2020; Maxwell et al., 2018). Concerns about the sustainability of large-scale ML applications justify this research.

We chose APS as a case study because the increasing presence of plastic in agri-food chains has raised significant environmental concerns due to plastic leakage and microplastics contamination (Ghaffar et al., 2022; Veettil et al., 2023; Zhang et al., 2025). However, mapping plastic-mulched

farmlands (PMF) and plastic greenhouses (PGH) is challenging due to the need for large datasets, clear imagery, and the high spectral similarity between APS and other targets (de Souza et al., 2024). There is demand for global APS maps that include small or sparse PGH and PMF structures (Fabrizi et al., 2025; Lu et al., 2025; Zhang et al., 2025; Tong et al., 2024), yet limited research has examined the suitability of individual satellite imagery sources for APS classification. Although the superior spatial resolution of PS enables the detection of smaller structures, its poorer spectral resolution (due to the absence of certain wavelengths) hampers the detection of plastic materials, creating a dilemma that warrants further examination. Our main contribution is to present results that promote this discussion. We do not include Landsat, the longest-running and most common satellite (Zhang et al., 2025; Hansen & Loveland, 2012), as a benchmark because its spatial resolution (30 m) is a significant limitation for detecting small or sparse APS.

2 Material and Methods

The methodology comprised five main stages: a Systematic Literature Review (SLR), sampling, data preparation, processing, and evaluation (see the Appendix for further details). We accessed multitemporal S2 imagery via the Google Earth Engine (GEE) API (Google, 2024) and downloaded PS imagery via the Planet Education and Research Program (Planet Labs PBC, 2024). Then, we generated a 3-time series with a 30-day mean composite for both satellites, following the method presented by de Souza et al. (2024).

The study area, encompassing two regions of interest (ROIs), is characterized by a high concentration of PMF and PGH in the metropolitan region of Campinas, São Paulo, Brazil. Each ROI has an area of approximately 330 km² (see Figure A.1).

The works of Basheer et al. (2024) and Tayer et al. (2023) have suggested testing two different band configurations for each satellite. First, we used all available PS and S2 bands with a spatial resolution of 20 meters or better, yielding eight PS and ten S2 bands. We then compared the satellites using the equivalent four bands: Red (R), Green (G), Blue (B), and Near Infrared (NIR), resulting in visible and NIR (VNIR). This VNIR configuration was intended to provide similar information from both satellite images, leaving the difference solely in spatial resolution and minor sensor variations. We employed pixel-based classification, testing seven ML classifiers selected via the SLR (see Appendix A.3) from the Scikit-Learn 1.3.2 Python library (Pedregosa et al., 2011). All classifiers used the default parameters and the same random state (2025).

We selected the most common metrics in the literature (see Table B.1), overall accuracy (OA) and Cohen's kappa (κ), together with training time (TT) and image classification time (ICT). TT and ICT denote the time spent fitting the model to the training set and the time required to predict an image, respectively. Additionally, we overlaid and visually inspected the most accurate classification results from each satellite (see Figure B.5). In the results, Table 1 presents the impact of replacing the image set from S2 to PS, showing differences in classification metrics (Eq. 1) and the relative changes in TT and ICT (Eq. 2). The difference (Δ) for the classification metrics, OA and κ, is defined in Equation 1.

$$\Delta M = M_{S2} - M_{PS} \tag{1}$$

Where M represents the metric being compared (either OA or κ). The relative change in processing time (t_{rel}), applicable to both TT and ICT, is calculated as indicated in Equation 2.

$$t_{\text{rel}} = \frac{t_{\text{PS}} - t_{\text{S2}}}{t_{\text{S2}}} = \frac{t_{\text{PS}}}{t_{\text{S2}}} - 1 \tag{2}$$

Where t_{PS} and t_{S2} represent the processing times for PlanetScope and Sentinel-2, respectively.

3 Results and Discussion

Figure 1 provides a summarized analysis of S2 and PS performance in APS mapping across multiple perspectives. By consolidating satellite imagery, algorithms, band configurations, and runtime into

a single, exploratory overview, this visualization highlights the overarching trade-off between accuracy and computational cost, especially when selecting the data source. Although interpreting this figure can be complex, it consolidates all the aspects considered in our comparison of PS and S2, enabling a comprehensive analysis. To supplement and individualize the analysis of each attribute, we included in the Appendix the figures B.1, which display separate graphs for 4 and all bands; B.2 exhibits ICT and TT relative change when switching satellites, and B.3 when varying the number of bands; B.4 shows OA and κ changes based on ML models and imagery sources. The individual Appendix graphs show mean values with error bars. The trend in metrics for each satellite remained consistent across band configurations, confirming the influence of the source (Fig. 1 and Table 1).

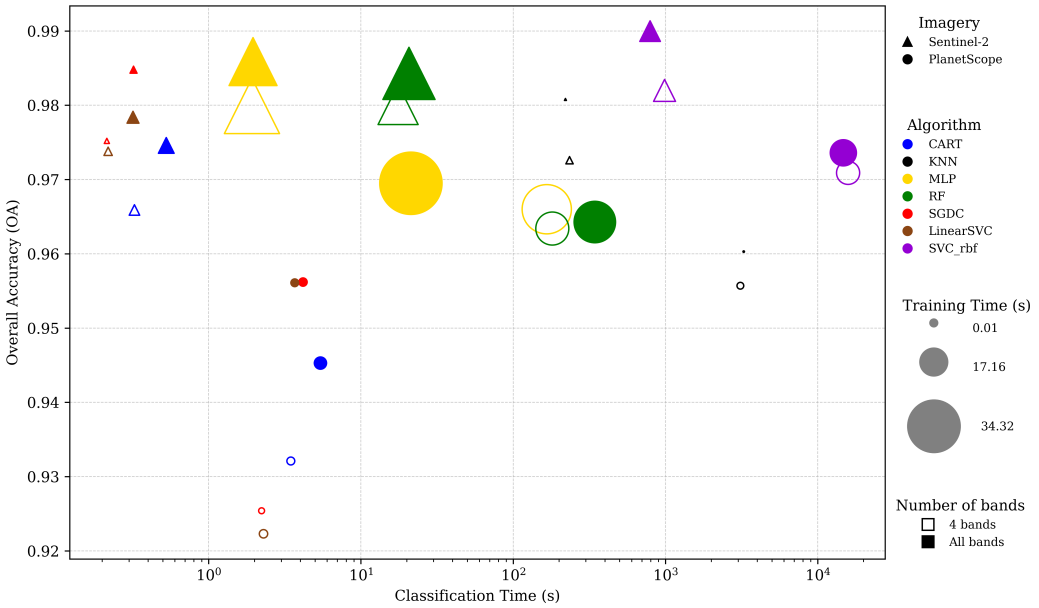

Figure 1: Accuracy and classification time (in logarithmic scale due to the extensive range) of the comparison between satellites, models, and the number of bands.

S2 imagery with 10 spectral bands achieved the highest OA and κ, and it outperformed PS across all algorithms analyzed (Fig. 1 and Table 1). On average, S2 had an OA 2.5% higher and a κ 3.7% higher than PS. Both image datasets showed longer times and improved accuracies for the sets with more bands (Fig. 1). PS consistently required more time to classify an image, and the runtime also increased with the algorithm's complexity (Table 1). The size of the image files accounts for the large difference in ICT. In the full-band configuration, although PS had fewer bands (8 *vs.* 10 of S2), the total number of pixels (across all bands) was 788% higher than in S2. The PS image (36.621.865 pixels x 8 bands x 3 times) had a file size four times larger than the S2 image of the same area (3.299.141 pixels x 10 bands x 3 times), and the additional data increased the PS ICT by nearly a factor of 10. The satellite did not affect the TT due to the methodological design employed.

The reasons for S2's superior performance are not entirely clear. It could be attributed to contributions from SWIR bands or to limitations in pixel-based classification. Non-visible spectral bands, such as SWIR, play a key role in APS mapping (Zhang et al., 2025; Veettil et al., 2023), but a definitive conclusion has not yet been reached. The higher spatial resolution of PS increased misclassification, particularly by increasing false positives (FP). In previous LCC studies, Rahman et al. (2020) conducted their work in an urban-dominated area and identified S2 as the most suitable imagery. In contrast, Acharki (2022); Rao et al. (2021); Ye et al. (2021) focused on ROIs dominated by agricultural and natural fields and concluded that PS was the best choice. However, in a broad literature review, Sheykhmousa et al. (2020) found that higher resolution reduced accuracy in many studies. Our results reinforce that while the worst spatial resolution of S2 may hinder the detection of small structures (false negatives), it could also reduce FP in pixel-based classification. The complex landscape of the study area leads to misclassifications in both satellite imagery, as shown in Appendix Figure B.5.

Table 1: Comparison of PlanetScope and Sentinel-2 performance across seven ML classifiers using four or full bands.

Imagery	Models	ΔOA (S2 – PS)	Δκ (S2 – PS)	TT relative change (%)	ICT relative change (%)
S2 *vs.* PS 4 bands	CART	0.0338	0.0508	-44%	964%
	kNN	0.0169	0.0254	-14%	1224%
	MLP	0.0139	0.0209	-20%	8531%
	RF	0.0167	0.0250	-32%	930%
	SGDC	0.0498	0.0747	32%	938%
	LinearSVC	0.0515	0.0773	2%	948%
	SVC rbf	0.0111	0.0166	11%	1504%
	Average 4 bands	0.0277	0.0415	-9%	2148%
S2 *vs.* PS 10 and 8 bands, respectively	CART	0.0293	0.0439	-40%	928%
	kNN	0.0205	0.0307	-41%	1380%
	MLP	0.0164	0.0246	69%	989%
	RF	0.0200	0.0299	-37%	1561%
	SGDC	0.0286	0.0430	39%	1199%
	LinearSVC	0.0223	0.0335	20%	1056%
	SVC rbf	0.0164	0.0246	61%	1759%
	Average full bands	0.0219	0.0329	10%	1267%

Discussion of computational costs and energy use in ML (García-Martín et al., 2019) is relevant to the sustainable production of global maps with sparse APS (Lu et al., 2025; Zhang et al., 2025). Over the past 20 years, advances in data availability and sensor integration have improved LCC, including APS remote mapping (Veettil et al., 2023). However, long-term, high-precision mapping remains challenging (Georganos et al., 2018; Zhang et al., 2025). Given PS's inferior performance and higher computational demands, S2 is preferable when using traditional ML. The case study was limited to a small area in the Brazilian interior. Scaling to the whole country, using the same computational power, would take 4 days with the fastest classifier (97.5% OA), and 5850 days (19 years) with the more accurate (99.0% OA). The 1.5% OA gain isn't worth the 1462.5-fold increase in runtime, making it impractical given that the APS lifespan is shorter than 19 years.

3.1 Limitations and future studies

Future studies should further investigate the factors that contributed to the results presented. Although S2 demonstrated superior performance, our methodological design did not incorporate deep learning models or hyperparameter optimization. Deep neural networks (DNNs) have achieved outstanding results in RS problems for some time (Zhang et al., 2025). Given that technologies are continually evolving in parallel, we are currently investigating deep architectures using the most recent satellite imagery as a continuation of this research. Such architectures require tuning to achieve optimal outcomes, which must also be included. We did not test DNNs because they require substantial training data, and we had a limited labeled sample.

4 Conclusion

Classifying RS images over large areas is computationally intensive and time-consuming. PS allocated more resources but did not achieve higher accuracy than S2 for APS mapping. We demonstrated the importance of an appropriate combination of datasets, algorithms, and computational resources for performing the target task. In line with the shift toward cost-effective solutions, we incorporated TT and ICT as relevant metrics. Among all tested configurations (satellite, bands, and model), S2 imagery with 10 multispectral bands and an MLP proved to be the most balanced in terms of computational cost, accuracy, and consistency.

We highlight the importance of considering classification quality and computational cost when selecting models and imagery. Previous studies have acknowledged SVM as the best algorithm for LC mapping, but none have evaluated its classification cost. In some tests, changing the algorithm had an effect on OA similar to changing the image set.

REFERENCES

Siham Acharki. Planetscope contributions compared to sentinel-2, and landsat-8 for lulc mapping. *Remote Sensing Applications: Society and Environment*, 27, 8 2022. ISSN 23529385. doi: 10.1016/j.rsase.2022.100774.

Siham Acharki and Bijeesh Kozhikkodan Veettil. Mapping plastic-covered greenhouse farming areas using high-resolution planetscope and rapideye imagery: studies from loukkos perimeter (morocco) and dalat city (vietnam). *Environmental Science and Pollution Research*, 30:23012–23022, 2 2023. ISSN 16147499. doi: 10.1007/s11356-022-23808-w.

Rama Akkiraju, Vibha Sinha, Anbang Xu, Jalal Mahmud, Pritam Gundecha, Zhe Liu, Xiaotong Liu, and John Schumacher. Characterizing machine learning processes: A maturity framework. In *Business Process Management*, volume 12168 of *Lecture Notes in Computer Science*, pp. 17–31, Cham, 2020. Springer. doi: 10.1007/978-3-030-58666-9_2.

Davide Andreatta, Damiano Gianelle, Michele Scotton, and Michele Dalponte. Estimating grassland vegetation cover with remote sensing: A comparison between landsat-8, sentinel-2 and planetscope imagery. *Ecological Indicators*, 141, 8 2022. ISSN 1470160X. doi: 10.1016/j.ecolind.2022.109102.

Alvin Balidoy Baloloy, Ariel Conferido Blanco, Christian Gumbao Candido, Reginal Jay Labadisos Argamosa, John Bart Lovern Caboboy Dumalag, Lady Lee Carandang DImapilis, and Enrico Camero Paringit. Estimation of mangrove forest aboveground biomass using multispectral bands, vegetation indices and biophysical variables derived from optical satellite imageries: Rapideye, planetscope and sentinel-2. In *ISPRS Annals of the Photogrammetry, Remote Sensing and Spatial Information Sciences*, volume 4, pp. 29–36. Copernicus GmbH, 4 2018. doi: 10.5194/isprs-annals-IV-3-29-2018.

Sana Basheer, Xiuquan Wang, Aitazaz A. Farooque, Rana Ali Nawaz, Kai Liu, Toyin Adekanmbi, and Suqi Liu. Comparison of land use land cover classifiers using different satellite imagery and machine learning techniques. *Remote Sensing*, 14, 10 2022. ISSN 20724292. doi: 10.3390/rs14194978.

Sana Basheer, Xiuquan Wang, Rana Ali Nawaz, Tianze Pang, Toyin Adekanmbi, and Muhammad Qasim Mahmood. A comparative analysis of planetscope 4-band and 8-band imageries for land use land cover classification. *Geomatica*, 76, 12 2024. ISSN 19254296. doi: 10.1016/j.geomat.2024.100023.

Joshua Braaten. Sentinel-2 cloud masking with s2cloudless, 2020. URL `https://developers.google.com/earth-engine/tutorials/community/sentinel-2-s2cloudless`. GitHub — Google for Developers.

A. G. Dalagan and J. A. Principe. Spatial inventory of solar photovoltaic (pv) installations using remote sensing and machine learning: Case of pampanga province, philippines. In *International Archives of the Photogrammetry, Remote Sensing and Spatial Information Sciences - ISPRS Archives*, volume 48, pp. 115–123. International Society for Photogrammetry and Remote Sensing, 3 2024. doi: 10.5194/isprs-archives-XLVIII-4-W9-2024-115-2024.

Marlon F de Souza, · R A C Lamparelli, · M H S Oliveira, · G P Nogueira, A Bliska, and T T Franco. Remote sensing detection of plastic-mulched farmland using a temporal approach in machine learning: case study in tomato crops. *Environmental Science and Pollution Research 2024*, pp. 1–14, 10 2024. ISSN 1614-7499. doi: 10.1007/S11356-024-35026-7.

Alessandro Fabrizi, Peter Fiener, Thomas Jagdhuber, Kristof Van Oost, and Florian Wilken. Plasticulture detection at the country scale by combining multispectral and sar satellite data. *Scientific Reports*, 15:1–19, 12 2025. ISSN 20452322. doi: 10.1038/S41598-025-93658-2.

Eva García-Martín, Crefeda Faviola Rodrigues, Graham Riley, and Håkan Grahn. Estimation of energy consumption in machine learning. *Journal of Parallel and Distributed Computing*, 134: 75–88, 12 2019. ISSN 07437315. doi: 10.1016/j.jpdc.2019.07.007.

M. Gašparović, D. Medak, I. Pilaš, L. Jurjević, and I. Balenović. Fusion of sentinel-2 and planetscope imagery for vegetation detection and monitoring. In *International Archives of the Photogrammetry, Remote Sensing and Spatial Information Sciences - ISPRS Archives*, volume 42, pp. 155–160. International Society for Photogrammetry and Remote Sensing, 9 2018. doi: 10.5194/isprs-archives-XLII-1-155-2018.

S. Georganos, T. Grippa, S. Vanhuysse, M. Lennert, M. Shimoni, S. Kalogirou, and E. Wolff. Less is more: optimizing classification performance through feature selection in a very-high-resolution remote sensing object-based urban application. *GIScience & Remote Sensing*, 55(2):221–242, 2018. doi: 10.1080/15481603.2017.1408892.

Imania Ghaffar, Muhammad Rashid, Muhammad Akmal, and Ali Hussain. Plastics in the environment as potential threat to life: an overview. *Environmental Science and Pollution Research*, 29: 56928–56947, 8 2022. ISSN 0944-1344. doi: 10.1007/s11356-022-21542-x.

Google. Google earth code editor, 2024. URL `https://earthengine.google.com/platform/`.

Matthew C. Hansen and Thomas R. Loveland. A review of large area monitoring of land cover change using landsat data. *Remote Sensing of Environment*, 122:66–74, 2012. ISSN 0034-4257. doi: 10.1016/j.rse.2011.08.024.

Marcin Kluczek, Bogdan Zagajewski, and Tomasz Zwijacz-Kozica. Mountain tree species mapping using sentinel-2, planetscope, and airborne hyspex hyperspectral imagery. *Remote Sensing*, 15, 2 2023. ISSN 20724292. doi: 10.3390/rs15030844.

Himanshu Kumar, Rohan Kumar, Sujay Dutta, and Magan Singh. Google's cloud computing platform-based performance assessment of machine learning algorithms for precisely maize crop mapping using integrated satellite data of sentinel-2a/b and planetscope. *Journal of the Indian Society of Remote Sensing*, 51:2599–2613, 12 2023. ISSN 09743006. doi: 10.1007/s12524-023-01764-3.

Dongwei Li, Shuliang Wang, Qiang He, and Yun Yang. Cost-effective land cover classification for remote sensing images. *Journal of Cloud Computing*, 11(1):62, 2022. doi: 10.1186/s13677-022-00335-0.

Yin Liu, Preeti Rao, Weiqi Zhou, Balwinder Singh, Amit K. Srivastava, Shishpal P. Poonia, Derek Van Berkel, and Meha Jain. Using sentinel-1, sentinel-2, and planet satellite data to map field-level tillage practices in smallholder systems. *PLoS ONE*, 17, 11 2022. ISSN 19326203. doi: 10.1371/journal.pone.0277425.

Lizhen Lu, Yunci Xu, Xinyu Huang, Hankui K. Zhang, and Yuqi Du. Large-scale mapping of plastic-mulched land from sentinel-2 using an index-feature-spatial-attention fused deep learning model. *Science of Remote Sensing*, 11:100188, 6 2025. ISSN 2666-0172. doi: 10.1016/J.SRS.2024.100188.

Júlia Matejčíková, Dana Vébrová, and Peter Surový. Comparative analysis of machine learning techniques and data sources for dead tree detection: What is the best way to go? *Remote Sensing*, 16, 8 2024. ISSN 20724292. doi: 10.3390/rs16163086.

Win Sithu Maung, Satoshi Tsuyuki, and Zhiling Guo. Improving land use and land cover information of wunbaik mangrove area in myanmar using u-net model with multisource remote sensing datasets. *Remote Sensing*, 16, 1 2024. ISSN 20724292. doi: 10.3390/rs16010076.

Aaron E. Maxwell, Timothy A. Warner, and Fang Fang. Implementation of machine-learning classification in remote sensing: an applied review. *International Journal of Remote Sensing*, 39: 2784–2817, 5 2018. ISSN 0143-1161. doi: 10.1080/01431161.2018.1433343.

Bill Herbert Ziegelmaier Neto, Marcos Benedito Schimalski, Veraldo Liesenberg, Camile Sothe, Rorai Pereira Martins-Neto, and Mireli Moura Pitz Floriani. Combining lidar and spaceborne multispectral data for mapping successional forest stages in subtropical forests. *Remote Sensing*, 16, 5 2024. ISSN 20724292. doi: 10.3390/rs16091523.

Vincent Wayuga Ogweno, Nathan Moore, and Dan Wanyama. Assessing cropland disagreement in tanzania using machine learning methods with sentinel-2 and planet scope imagery. *International Journal of Remote Sensing*, 44:6716–6735, 2023. ISSN 13665901. doi: 10.1080/01431161.2023.2274320.

Matthew J. Page, Joanne E. McKenzie, Patrick M. Bossuyt, Isabelle Boutron, Tammy C. Hoffmann, Cynthia D. Mulrow, Larissa Shamseer, Jennifer M. Tetzlaff, Elie A. Akl, Sue E. Brennan, Roger Chou, Julie Glanville, Jeremy M. Grimshaw, Asbjørn Hróbjartsson, Manoj M. Lalu, Tianjing Li, Elizabeth W. Loder, Evan Mayo-Wilson, Steve McDonald, Luke A. McGuinness, Lesley A. Stewart, James Thomas, Andrea C. Tricco, Vivian A. Welch, Penny Whiting, and David Moher. The PRISMA 2020 statement: an updated guideline for reporting systematic reviews. *BMJ*, 372: n71, 2021. doi: 10.1136/bmj.n71.

Fabian Pedregosa, Gaël Varoquaux, Alexandre Gramfort, Vincent Michel, Bertrand Thirion, Olivier Grisel, Mathieu Blondel, Peter Prettenhofer, Ron Weiss, Vincent Dubourg, Jake Vanderplas, Alexandre Passos, David Cournapeau, Matthieu Brucher, Matthieu Perrot, and Édouard Duchesnay. Scikit-learn: Machine learning in python. *Journal of Machine Learning Research*, 12:2825–2830, 2011. ISSN 1533-7928. URL `http://jmlr.org/papers/v12/pedregosa11a.html`.

Planet Labs PBC. Education and research. `https://www.planet.com/industries/education-and-research/`, 2024. Accessed: 2026-02-03.

Ashikur Rahman, Hasan Muhammad Abdullah, Md Tousif Tanzir, Md Jakir Hossain, Bhoktear M. Khan, Md Giashuddin Miah, and Imranul Islam. Performance of different machine learning algorithms on satellite image classification in rural and urban setup. *Remote Sensing Applications: Society and Environment*, 20, 11 2020. ISSN 23529385. doi: 10.1016/j.rsase.2020.100410.

Preeti Rao, Weiqi Zhou, Nishan Bhattarai, Amit K. Srivastava, Balwinder Singh, Shishpal Poonia, David B. Lobell, and Meha Jain. Using sentinel-1, sentinel-2, and planet imagery to map crop type of smallholder farms. *Remote Sensing*, 13, 5 2021. ISSN 20724292. doi: 10.3390/rs13101870.

Mohammadreza Sheykhmousa, Masoud Mahdianpari, Hamid Ghanbari, Fariba Mohammadimanesh, Pedram Ghamisi, and Saeid Homayouni. Support vector machine versus random forest for remote sensing image classification: A meta-analysis and systematic review. *IEEE Journal of Selected Topics in Applied Earth Observations and Remote Sensing*, 13:6308–6325, 2020. ISSN 21511535. doi: 10.1109/JSTARS.2020.3026724.

Thiaggo C. Tayer, Michael M. Douglas, Maurício C.R. Cordeiro, André D.N. Tayer, J. Nik Callow, Leah Beesley, and Don McFarlane. Improving the accuracy of the water detect algorithm using sentinel-2, planetscope and sharpened imagery: a case study in an intermittent river. *GIScience and Remote Sensing*, 60, 2023. ISSN 15481603. doi: 10.1080/15481603.2023.2168676.

Xiaoye Tong, Xiaoxin Zhang, Rasmus Fensholt, Peter Rosendal Dau Jensen, Sizhuo Li, Marianne Nylandsted Larsen, Florian Reiner, Feng Tian, and Martin Brandt. Global area boom for greenhouse cultivation revealed by satellite mapping. *Nature Food*, 5:513–523, 5 2024. ISSN 2662-1355. doi: 10.1038/s43016-024-00985-0.

Bijeesh Kozhikkodan Veettil, Dong Doan Van, Ngo Xuan Quang, and Pham Ngoc Hoai. Remote sensing of plastic-covered greenhouses and plastic-mulched farmlands: Current trends and future perspectives. *Land Degradation & Development*, 34:591–609, 2 2023. ISSN 1085-3278. doi: 10.1002/ldr.4497.

Marco Vizzari. Planetscope, sentinel-2, and sentinel-1 data integration for object-based land cover classification in google earth engine. *Remote Sensing*, 14, 6 2022. ISSN 20724292. doi: 10.3390/rs14112628.

João P.S. Werner, Mariana Belgiu, Inacio T. Bueno, Aliny A. Dos Reis, Ana P.S.G.D. Toro, João F.G. Antunes, Alfred Stein, Rubens A.C. Lamparelli, Paulo S.G. Magalhães, Alexandre C. Coutinho, Júlio C.D.M. Esquerdo, and Gleyce K.D.A. Figueiredo. Mapping integrated crop–livestock systems using fused sentinel-2 and planetscope time series and deep learning. *Remote Sensing*, 16, 4 2024. ISSN 20724292. doi: 10.3390/rs16081421.

Ning Ye, Justin Morgenroth, Cong Xu, and Na Chen. Indigenous forest classification in new zealand – a comparison of classifiers and sensors. *International Journal of Applied Earth Observation and Geoinformation*, 102, 10 2021. ISSN 1872826X. doi: 10.1016/j.jag.2021.102395.

Bogdan Zagajewski, Marcin Kluczek, Karolina Barbara Zdunek, and David Holland. Sentinel-2 versus planetscope images for goldenrod invasive plant species mapping. *Remote Sensing*, 16, 2 2024. ISSN 20724292. doi: 10.3390/rs16040636.

Mengmeng Zhang, Jinwei Dong, Quansheng Ge, Hasituya, and Pengyu Hao. A review of agricultural film mapping: Current status, challenges, and future directions. *Journal of Remote Sensing*, 5, 1 2025. ISSN 2694-1589. doi: 10.34133/remotesensing.0395.

ACKNOWLEDGMENT

Braskem S.A. and the São Paulo Research Foundation (FAPESP) financed this work within the Plasticulture Engineering Center (grant numbers: 2021/05251-8; 2024/06854-6; 2024/06856-9). Author R.A.C. Lamparelli received financial support from the Brazilian National Council for Scientific and Technological Development – CNPq (grant number 305412/2023-0). Author M.H.S. Oliveira has received research support from PIBIC/CNPq (grant no. 125120/2023–0) and Dow Ilimite-se/Unicamp (grant no. 01-P-416/2024).

CODE AND DATA AVAILABILITY

The implementation code used in this study is publicly available in the following repository: `https://github.com/MuriloHSO/Beyond-Spatial-Resolution-Code`.

APPENDIX

A DETAILS ABOUT MATERIAL AND METHODS

A.1 SYSTEMATIC LITERATURE REVIEW

The SLR adhered to the Preferred Reporting Items for Systematic Reviews and Meta-Analyses (PRISMA) statement (Page et al., 2021). We looked for studies comparing PS and S2 imagery collections in the Web of Science and Scopus scientific databases. The search query used was ((”PlanetScope” OR ”Planet Scope” OR ”PS”) AND (”Sentinel-2” OR ”Sentinel 2” OR ”S2”) AND (”classification performance” OR ”classification accuracy” OR ”image classification”)). The search was conducted on May 8th, 2025, limited to the topic in WoS and the similar ”Title, abstract, and keywords” in Scopus. After removing duplicate results, this process identified 61 unique papers. Then, we screened the titles and abstracts, excluding 34 papers. Additionally, three articles not focused on satellite comparison were excluded during the full-text eligibility assessment. The final 18 articles, along with their respective best-performing satellites, were listed in Table B.1. We also documented the algorithms tested, the accuracy metrics used for assessment, whether human visual inspection of results was employed, and the relevance to APS mapping.

A.2 DATA AND SAMPLING

The study area with the two regions of interest (ROI) is shown in Figure A.1. ROIs covered areas with a high concentration of PMF and PGH in the metropolitan region of Campinas, São Paulo, Brazil. Each ROI (around 330 km²) was divided in half, with training and testing data on the left and validation data on the right, as indicated in Figure A.1.

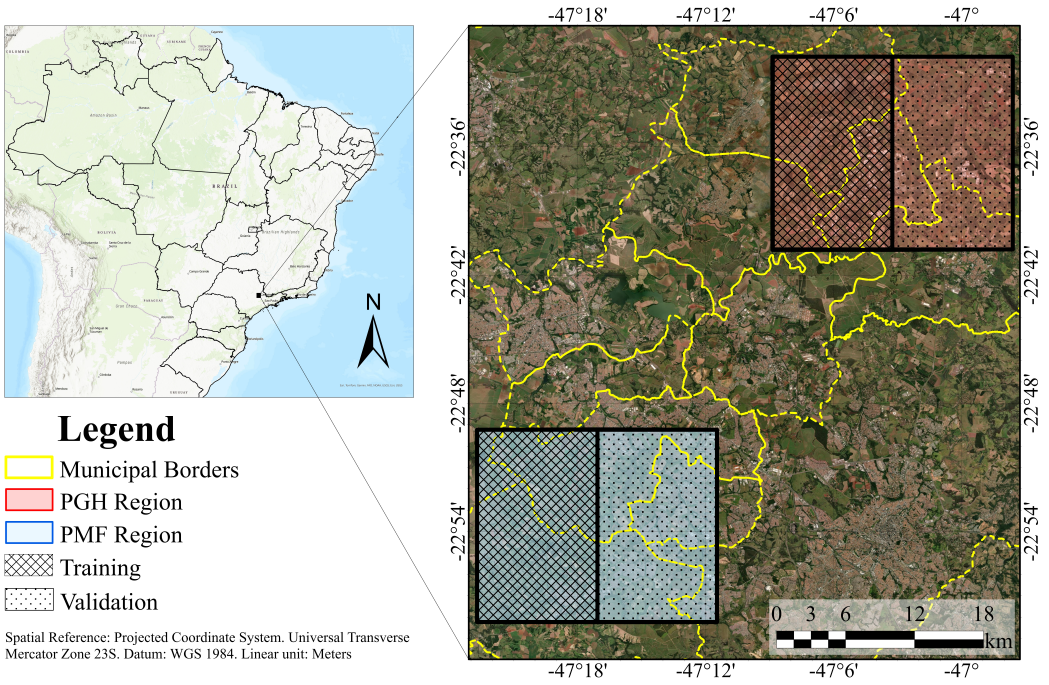

Figure A.1: Regions of Interest (ROIs) selected based on the occurrence of PGH and PMF.

The streamlined time series (de Souza et al., 2024) reduced dependence on temporal resolution. The PS image set had enough clear images. On the other hand, for S2 imagery, we defined a maximum of 50% cloud coverage and applied the s2cloudless (Braaten, 2020) cloud mask before assembling subsets and generating a 30-day mean composite.

Polygons were labeled within the ROIs based on field visits and desk delineation through visual observation of very high-resolution (0.3 m) satellite images. These polygons were classified into

three categories: PMF, PGH, and others. Subsequently, we generated random points within polygons and extracted labels and spectral information for each class from the S2 and PS (Table A.1). Each randomly generated point within the training and validation polygons acted as a geographic anchor to directly sample the spectral value from the native grid of each satellite. This point-to-pixel approach ensured that models were trained on the original sensor data without the artifacts or information loss associated with spatial resampling or downscaling. The data was standardized using *"StandardScaler()"* from sklearn.preprocessing.

Table A.1: PS and S2 selected bands and spectral information.

	PlanetScope (PSB.SD)			**Sentinel 2 (MSI)**		
Band name	Pixel size (m)	Wavelength (nm)	Description	Pixel size (m)	Wavelength (nm)	Description
B1	3	431 - 452	Coastal Blue	-	-	-
B2	3	465 - 515	Blue	10	492.1 - 496.6	Blue
B3	3	513 - 549	Green I	10	559 - 560	Green
B4	3	547 - 583	Green	10	664.5 - 665	Red
B5	3	600 - 620	Yellow	20	703.8 - 703.9	Red Edge 1
B6	3	650 - 680	Red	20	739.1 - 740.2	Red Edge 2
B7	3	697 - 713	Red Edge	20	779.7 - 782.5	Red Edge 3
B8	3	845 - 885	NIR	10	833 - 835.1	NIR
B8A	-	-	-	20	864 - 864.8	Red Edge 4
B11	-	-	-	20	1610 - 1614	SWIR 1
B12	-	-	-	20	2185 - 2202	SWIR 2

A.3 Model training

The seven supervised ML classifiers from Scikit-Learn 1.3.2 (Pedregosa et al., 2011) tested were: Classification And Regression Tree (CART), k-Nearest Neighbors (kNN), MultiLayer Perceptron (MLP), Random Forest (RF), and Support Vector Classifier (SVC) with Radial Basis Function (RBF) kernel, henceforth called $SVCrbf$. Due to the longer classification time of $SVCrbf$, we incorporated the Stochastic Gradient Descent Classifier with linear SVM (SGDC) and the LinearSVC to improve the discussion.

B Supplementary Results

B.1 Systematic Literature Review

The final articles included in the SLR (Table B.1) employed a diverse range of remote sensing datasets beyond PS and S2, along with various classification algorithms and accuracy metrics. The comparison of imagery sources included very-high-spatial-resolution optical sensors in satellites, such as WorldView-2 (WV2) and CBERS-4A, high-resolution like RapidEye (RE), as well as medium-resolution sensors such as Landsat-8 (L8). In addition, the Sentinel-1 (S1) radar sensor, aerial imagery from drones and aircraft, and fused or sharpened imagery were included. Classification models predominantly used RF and SVM, with recent studies integrating DL architectures such as Convolutional Neural Networks (CNN). Some articles have employed specific models for target detection, such as the Fractional Response Model (FRM) for estimating grassland Fractional Vegetation Cover (Andreatta et al., 2022) and the Water Detect algorithm (WDA) by Tayer et al. (2023). Accuracy assessments primarily relied on OA and κ, supplemented in some cases by metrics such as Precision (P), Recall (R), F1-Score (F1), Intersection over Union (IoU), and Matthews Correlation Coefficient (MCC). The combination of PS and SVM was frequently identified as yielding the most robust classification performance, with RF also demonstrating consistent results across multiple studies.

Hitherto, we have not found studies that have evaluated TT and ICT, leaving a gap in understanding the trade-off between accuracy and runtime. Only the work of Acharki (2022) compared different image collections alongside APS mapping.

Table B.1: The final articles from the SLR, along with the metrics employed, the imagery collections compared, the best-performing satellite, the models tested, and the most effective algorithm.

Article	Metrics	Imagery collections compared	Best imagery**	Algorithms tested	Best algorithm*	Visual inspection
Baloloy et al. (2018)	R^2	PS, S2, RE	RE	Different regressions	MARS	Yes
Gašparović et al. (2018)	OA, κ	PS, S2, fusion	PS	RF	–*	Yes
Rahman et al. (2020)	OA, κ	L8, PS, S2	S2	RF, SVM, STACK	SVM	Yes
Rao et al. (2021)	OA, R, P, F1	PS, S1, S2	PS	SVM	–	Yes
Ye et al. (2021)	OA, R, P, κ	PS, S2, WV2, fusion	PS	SVM, RF, NN	SVM	Yes
Acharki (2022)	OA, κ, F1	L8, PS, S2, fusion	PS	RF	–*	Yes
Andreatta et al. (2022)	R^2	L8, PS, S2	S2	FRM	–*	Yes
Basheer et al. (2022)	OA, κ	L8, PS, S2	PS	SVM, RF, RT, CART	SVM	Yes
Liu et al. (2022)	OA	PS, S1, S2	PS	RF	–*	No
Vizzari (2022)	OA, R, P, F1	PS, S1, S2, fusion	S2	RF	–*	Yes
Acharki & Veettil (2023)	OA, κ, F1	PS, S1, S2, RE, fusion	S2	SVM, RF	SVM	Yes
Dalagan & Principe (2024)	P, R, F1, κ, OA	PS, S1, S2	S2	SVM, RF, NB	SVM	Yes
Kluczek et al. (2023)	F1	PS, S2, airborne hyperspectral	S2	SVM, RF	RF	Yes
Kumar et al. (2023)	OA, κ	PS, S2, fusion	PS	CART, RF, SVM	CART	Yes
Maung et al. (2024)	OA, IoU, F1, P, R	PS, S2, fusion	PS	U-Net, ANN	U-Net	Yes
Ogweno et al. (2023)	OA, κ	PS, S2	PS	CART, RF, SVM	RF	Yes
Tayer et al. (2023)	MCC	PS, S2, SVNIR	PS (4 bands)	WDA	–*	Yes
Neto et al. (2024)	κ	CBERS-4A, L8, PS, S2	S2	RT, SVM, MLC	SVM	Yes
Basheer et al. (2024)	OA, κ	PS (4 or 8 bands)	PS (8 bands)	SVM, ML, RF, KNN	SVM	Yes
Matejčíková et al. (2024)	OA	Aerial images, PS, S2	S2	RF, CNN	CNN	Yes
Werner et al. (2024)	OA, F1, R, P	PS, S2, fusion	S2	RF, TempCNN, ResNet, L-TAE	TempCNN	Yes
Zagajewski et al. (2024)	F1	PS, S2	S2	SVM, RF	RF	Yes

* Single-algorithm studies

** Disregarding fusion or sharpening

B.2 Individual outcomes of the aspects analyzed when comparing PS and S2

Figure B.1 compares the satellites, presenting band configuration separately to reduce information overload (from Figure 1 in the main text) and improve analysis. In B.1.a, we display the four equivalent bands (R, G, B, and NIR), and in B.1.b, all the bands selected for each satellite. Results indicate that fewer bands lead to reduced accuracy.

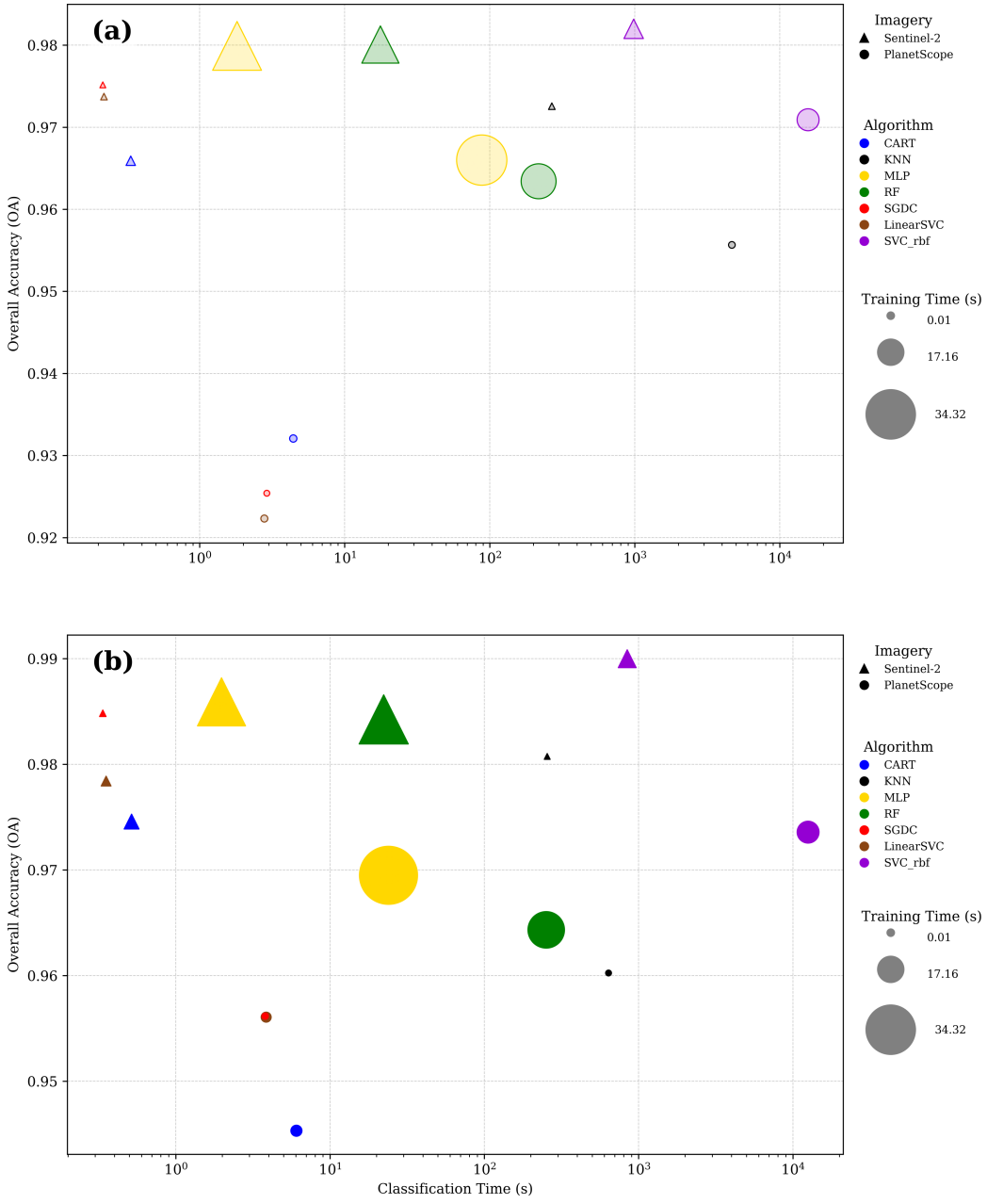

Figure B.1: (a) OA and ICT (log scale) for 4 equivalent bands of S2 and PS. b) OA and ICT (log scale) for all selected bands.

We measured time (TT and ICT) and classification accuracy (OA and κ) using 10-fold cross-validation on the dataset, with a random state of 2025. Figure B.2 illustrates the relative variations of TT and ICT with the change from satellite S2 to PS, and Figure B.3 illustrates the relative variations in TT and ICT due to the increase in the number of bands. The result showed that the dataset

change caused minimal or no variation in TT, while a substantial increase in ICT was observed, particularly for $SVCrbf$ and MLP, the latter also showed large error deviation. Moreover, the impact of the number of bands varies considerably across models, with no consistent trend and substantial deviations in the results. TT exhibits the most pronounced changes, including increases for CART and LinearSVC and reductions for KNN. In contrast, ICT times are less affected by changes in band configuration.

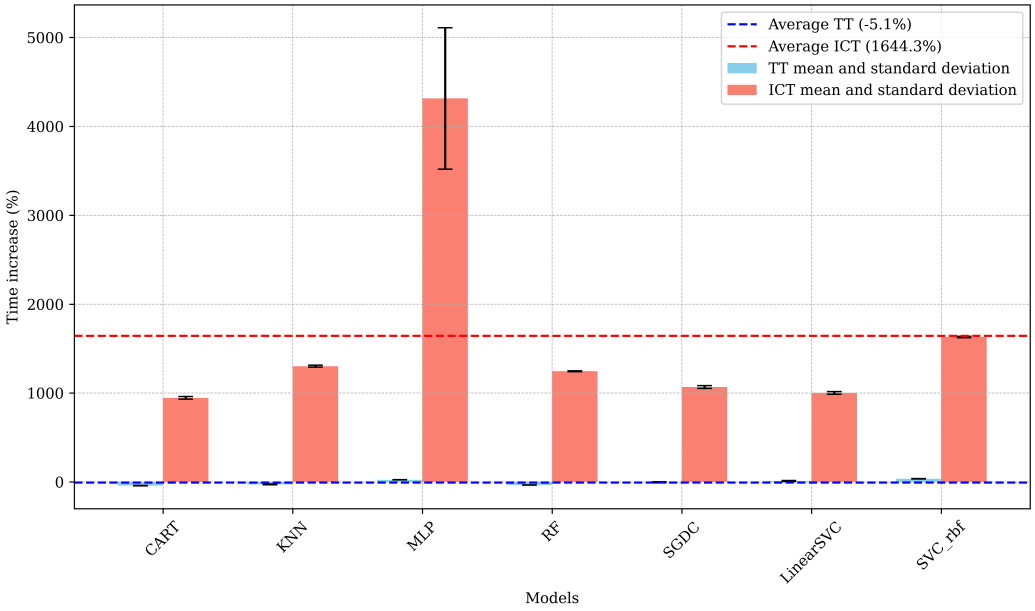

Figure B.2: Relative change of TT and ICT when switching from S2 to PS imagery.

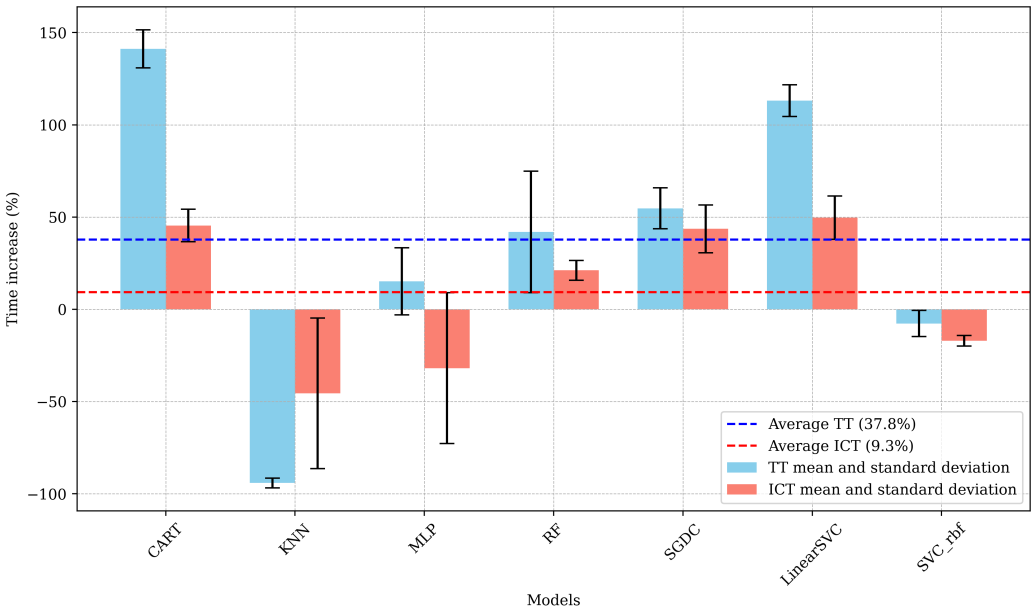

Figure B.3: Relative change of TT and ICT due to the increase in the number of bands.

Figure B.4 presents the classification performance, specifically (a) OA and (b) κ, accompanied by their respective error bars derived from the 10-fold cross-validation results. The metrics exhibit minimal variation, indicating high model stability across all folds.

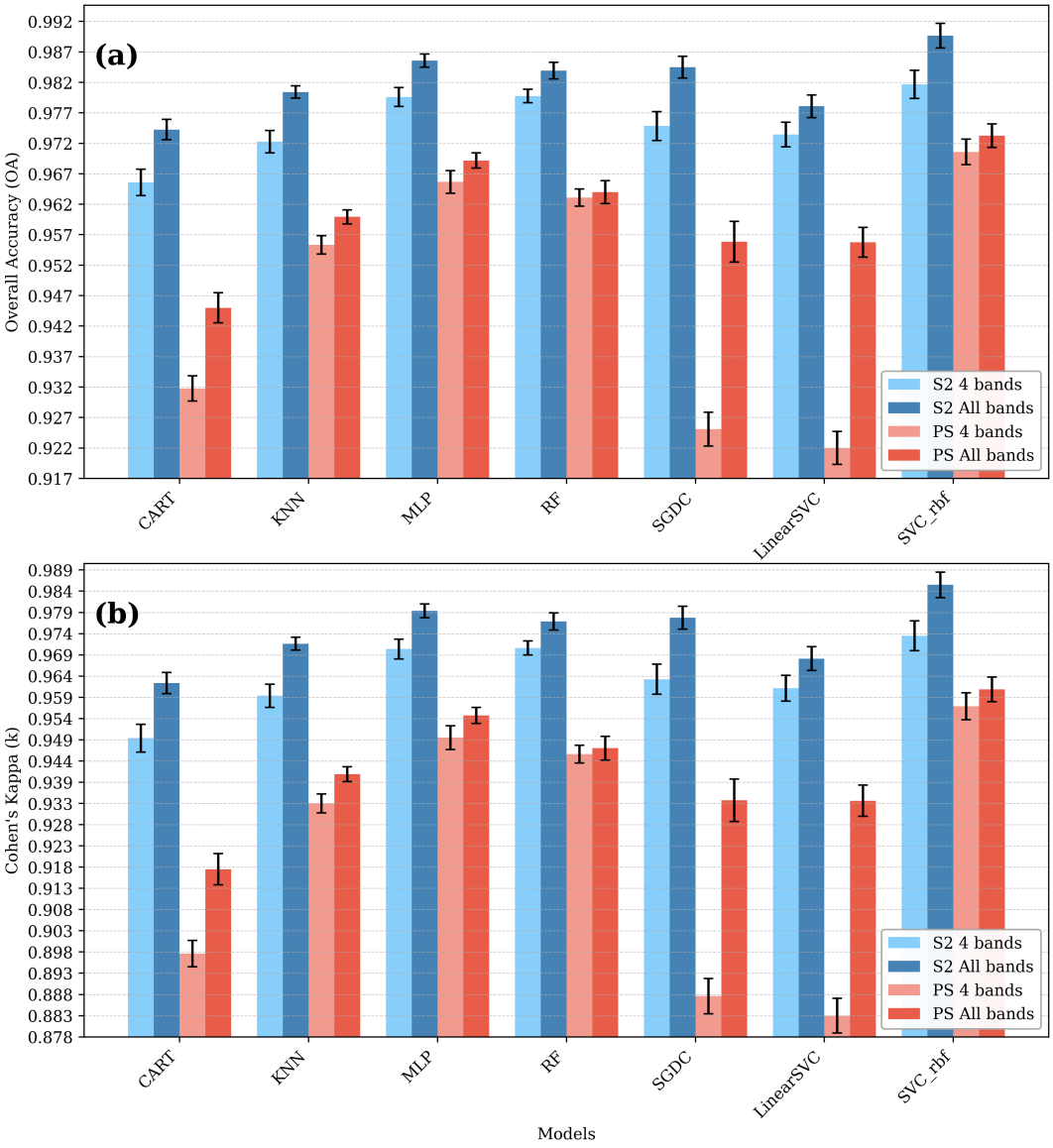

Figure B.4: Classification metrics variations according to ML model, including (a) Overall accuracy (OA) and (b) Cohen's Kappa (κ). Mean values with error bars for S2 and PS, with either four equivalent bands or all selected bands.

B.3 Visual inspection: Scene Complexity and Performance

The study area has a complex landscape, resulting in misclassification for both satellites. The differences in classification between S2 and PS are shown in Figure B.5. In the PMF area (Fig. B.5A), PS allowed the identification of finer details between planting rows that S2 could not capture. Figure B.5B indicates, within the pink circles, a higher occurrence of false positives (FP) of urban structures classified as PGH, mainly with PS. False negatives (FN) from S2 can be observed inside the purple circles in Figures B.5B and B.5D. In the region delimited by the yellow circle (Fig. B.5C), PS showed a greater occurrence of FP compared to S2, misclassifying urban areas as PGH. Some roofing materials used in large warehouses, or even the paints used to coat these roofs, may contain polymers (commonly called plastics) in their composition, complicating the classification. The green-circled region in Figure B.5D shows PS FP between houses and PGH. Almost all areas classified as PGH by S2 were also captured by PS. However, PS introduced many additional FP, while S2 had some FN.

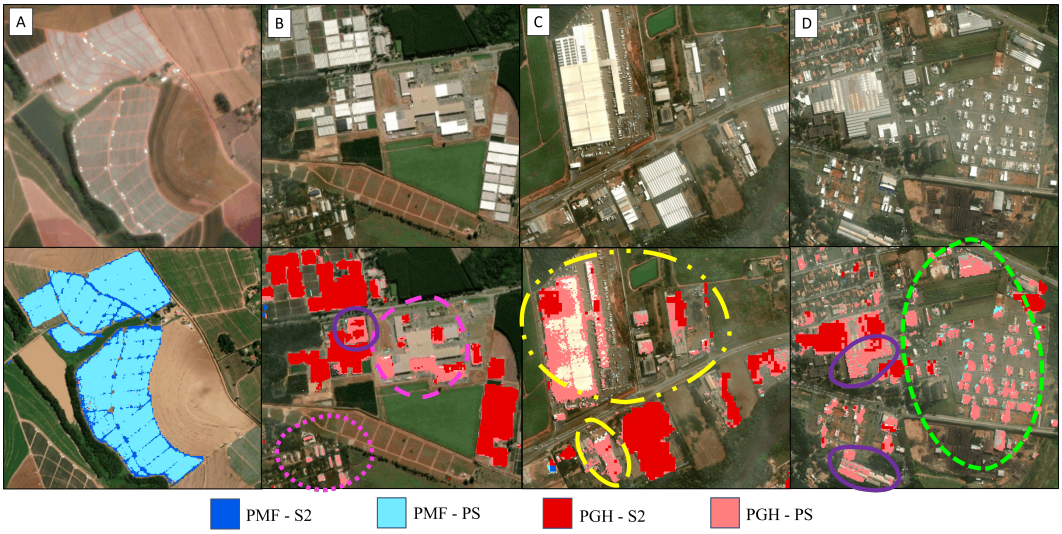

Figure B.5: Visual inspection of the APS classification results of S2-10 bands and PS-8 bands, both with SVC rbf and using satellite RGB base map.